Proteomics

WILEY-VCH

SPECIAL ISSUE Ion Mobility-Mass Spectrometry in Omics

Proteomics
Proteomics and Systems Biology

RESEARCH ARTICLE OPEN ACCESS

High-Resolution Ion Mobility as an Alternative to Quadrupole-Based Precursor Isolation for Reducing Chimeric Fragmentation Spectra in Bottom-Up Proteomics

Isabel R. Uribe | Liulin Deng | Leonard Rorrer III | Lauren Royer | Miriam Fico | Daniel DeBord

MOBILion Systems, Inc., Chadds Ford, Pennsylvania, USA

Correspondence: Daniel DeBord (daniel.debord@mobilionsystems.com)

Received: 18 May 2025 | **Revised:** 4 November 2025 | **Accepted:** 10 November 2025

ABSTRACT

To assess the potential for high resolution ion mobility (HRIM) as an alternative means of precursor isolation for mass spectrometry fragmentation analysis we performed a meta-analysis of predicted tryptic peptide features from the human proteome to measure the rate of chimeric spectrum generation relative to traditional quadrupole-based isolation. Results indicate that for proteomic mixtures, HRIM separation with a peak capacity of 100 produces chimeric spectra at a rate commensurate with a ~5 Th quadrupole isolation window, while providing the additional benefit of generating non-chimeric spectra for many isobaric and isomeric peptides unresolvable with a quadrupole filter. This behavior was verified experimentally using a HRIM-QTOF mass spectrometry system. The ability to combine HRIM and MS isolation resulted in >10× increase in precursor isolation specificity as compared to either of the techniques independently.

1 | Introduction

Tandem high resolution mass spectrometry (HRMS) has become a cornerstone of proteomics research for uncovering the complexities of biological systems [1–3]. Essential to bottom-up proteomics is accurate identification of peptides from their characteristic fragmentation patterns via tandem MS (MS/MS) experiments. Liquid chromatography (LC) is usually employed to separate peptides and reduce the number of peptides introduced to the mass spectrometer at a given time. However, the millions of unique peptides present in typical biological samples mean that complete separation by LC is impossible, necessitating ion fragmentation analysis to selectively identify and quantify as many peptides and proteins as possible. Since virtually all tandem MS systems today employ a quadrupole mass analyzer to isolate peptide precursors, any co-eluting peptides that are similar in m/z are co-isolated within the same m/z window, resulting in MS/MS spectra that contain fragment ions from all co-isolated peptides (termed chimeric spectra). The resulting spectral convolution makes it challenging to differentiate which fragment ions belong to which precursor, thereby diminishing the efficiency and accuracy of peptide identifications based on MS/MS [4, 5]. It is well known that the primary means of reducing the rate of chimeric spectral generation is to reduce the size of the m/z window used for precursor isolation, with the practical limit for quadrupole analyzers being ~0.7 Th, corresponding to the ability to isolate a single isotopic peak within a doubly charged peptide isotope distribution. However, ultra narrow quadrupole isolation windows limit ion transmission of the target species by up to 90% [6], reducing the sensitivity of analysis. For this reason, most researchers use more modest isolation windows of 1.5–4 Th, but even for this level of selectivity, hundreds of isolation events are required to cover the proteomics m/z range of interest (approximately m/z 400–1000) in the oft preferred data independent acquisition (DIA) mode of operation. This means that a reduced precursor mass range must be used or extended MS1/MS2 cycle times (MS1 = precursor ion scan, MS2 = fragment ion scan) result in insufficient sampling across LC peaks. Additionally, cycling

through hundreds of isolation windows means each window can only be sampled for a short period of time, leading to ion utilization rates as low as 0.5%, which limits MS2 sensitivity [7]. And still, as many as 39% of MS2 spectra are predicted to be chimeric, even when acquired with a narrow 2 Th quadrupole isolation window [8]. Researchers have expended significant effort exploring various methods of optimizing quadrupole isolation to minimize tradeoffs between selectivity, speed, sensitivity, and mass range for specific proteomics workflows, and this work has shown that when employing only m/z-based precursor isolation, the speed of the quadrupole analyzer is a fundamental metric which drives performance, enabling the sampling of more windows with higher selectivity per scan cycle [9]. Most modern instruments employing DIA with quadrupole-only precursor selection employ mass selection windows in the range of 2–20 Th [9]. In cases where selectivity and identification confidence are prioritized over the DIA benefits of unbiased analysis and greater data completeness, data dependent acquisition (DDA) can enable access to narrower quadrupole windows with extended dwell times for higher quality fragmentation spectra, albeit for a reduced number of target analytes.

This reality of imperfect precursor isolation has long been recognized and researchers have therefore developed several computational approaches to enable reliable identification of co-fragmented precursors from chimeric spectra [5, 8, 10–12], both for DDA data [5, 8, 10], and DIA data [10, 13]. In typical use, these tools enable multiplexed peptide identification able to routinely identify upwards of 2–6 peptides in a given spectrum [5, 8, 12, 14], but this is highly dependent on factors such as the relative abundances of the precursors, the number and abundance of particular peptide fragmentation spectra, whether the specific precursors are included in the search space, and the mass resolution of the instrument employed. However, despite advancements over the past couple decades, there is a limit to the spectral complexity that any tool can manage and finding ways to reduce chimerism without sacrificing speed, sensitivity, or range of analysis is anticipated to benefit any downstream processing approach employed.

Ion mobility (IM) represents a potential solution to mitigate the chimeric overlap resulting from quadrupole-based precursor isolation with added benefits of increased speed and sensitivity for ion fragmentation [15, 16]. As a high-speed separations technique which operates on a time scale faster than LC but slower than time of flight (TOF) mass spectrometry, IM acts as an additional online separation that further isolates precursors from each other prior to fragmentation analysis, resulting in cleaner fragmentation spectra than can be achieved by LC-MS/MS alone. Additionally, since IM separates ions based on size to charge ratios rather than m/z, many species that are inseparable by quadrupole filtering (e.g., isomers and isobars) can easily be resolved by ion mobility. IM has been applied to ion fragmentation analysis of proteomic mixtures with varying degrees of success over the years [13, 15–23]. Most recently, the line of timsTOF mass spectrometers introduced by Bruker Daltonics (Billerica, Massachusetts) has revolutionized the field of proteomics by demonstrating the benefits of IM-enhanced ion fragmentation analysis. By leveraging the trapped ion mobility spectrometry (TIMS) technology to supplement quadrupole isolation, significant gains in the speed and sensitivity of MS2 spectra generation have been realized, especially considering the capability to store up precursor ions while previous ions are being analyzed (i.e., parallel accumulation) [13]. Further testing using the TIMS separation for precursor isolation without additional quadrupole filtering has been shown to generate chimeric spectra at a rate equivalent to a 12.5 Th quadrupole isolation window, meaning it is less selective than many quadrupole-based DIA approaches [23]. For this reason, researchers have primarily employed TIMS in conjunction with quadrupole isolation, where it has the effect of reducing the effective Q1 isolation window by a factor of 4 in terms of the chimeric spectral generation rate [23]. As a result, wider m/z isolation windows can be used to achieve faster cycle times and greater ion utilization without sacrificing selectivity in precursor isolation.

With the undeniable impact the TIMS parallel accumulation serial fragmentation (PASEF) approach has had on proteomics analysis, an obvious direction for further improvement is to evaluate whether a higher resolution ion mobility separation might further extend the performance profile in one or more areas. Structures for Lossless Ion Manipulation (SLIM) represents a next generation high-resolution ion mobility (HRIM) technique that utilizes ultra long mobility separation path lengths and traveling wave ion mobility spectrometry (TWIMS) to enhance gas phase ion separation [24, 25]. A SLIM-QTOF instrument therefore has potential to translate this greater separation capability into improved ion fragmentation analysis performance [7, 26, 27], but the rate of chimeric spectra generation by a SLIM-QTOF has yet to be quantitatively assessed. Here, we examine the number of chimeric precursors predicted to form during simulated quadrupole- and HRIM-based isolation of unmodified tryptic peptides predicted from the human proteome, along with supporting examples from experimental data.

2 | Methods

2.1 | Creating a Database of Peptides and Their Predicted Properties

Prediction of tryptic peptide sequences and their corresponding precursor m/z, charge state (z), and normalized retention time (RT) (Table S1) was performed using pre-trained models in the publicly available AlphaPeptDeep (PeptDeep) [28] (Figure 1). In the "Model" tab of the PeptDeep graphic user interface (GUI), the pre-loaded default settings were utilized except "timsTOF" was used as the instrument parameter. In the "Library" tab of the PeptDeep GUI, pre-loaded default settings were utilized except the input FASTA file contained the human proteome (Uniprot ID UP000005640 including isoforms and reviewed sequences only, downloaded on January 29, 2025) and the resulting predicted library was written in a TSV file format that can be read by the DIA-NN and Spectronaut software programs. The resulting peptide library from the PeptDeep GUI contained predicted precursor m/z, z, apex RT, and the expected m/z values for predicted b and y peptide fragment ions. Predicted apex CCS and z values for tryptic peptides from the human proteome were obtained from a supplementary data table, which contained 616,948 unique peptide sequences predicted using the publicly available pre-trained DeepCollisionalCrossSection (DeepCCS) model (Figure 1), as previously described [29].

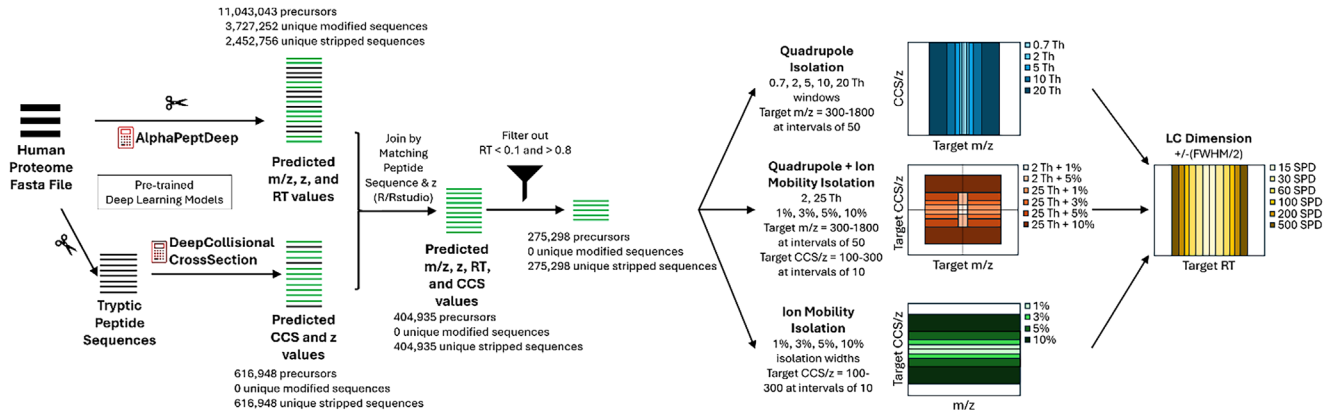

FIGURE 1 | Schematic workflow for in silico peptide database generation and downstream analysis in R. A human proteome FASTA file is digested into tryptic peptide sequences, which are then processed using deep learning-based predictive models: AlphaPeptDeep estimates mass to charge (m/z), charge state (z), and retention time (RT), while DeepCollisionalCrossSection predicts collisional cross section (CCS) and z values. The predicted peptide properties are merged to generate a comprehensive peptide database containing m/z, z, RT, and CCS/z for each sequence. These data are used to simulate proteomics experiments under various instrument acquisition modes: quadrupole-only, quadrupole + ion mobility (IM), and IM-only. Resulting peptide distributions are visualized across the m/z, CCS/z, and RT dimensions.

The peptide libraries resulting from the PeptDeep and DeepCCS deep learning models contained different numbers of peptides due to the parameters assumed for trypsin digestion of the human proteome (Table S1). The two peptide libraries were combined in R (Figure 1) by matching values for the peptide sequence and the associated precursor charge state (z). The final library (Table S2) contained 404,935 unmodified peptides and their predicted m/z, z, RT, and CCS/z values (Figure 1).

2.2 | Informatics Analysis of Chimeric Precursor Groups Predicted Under Various Experimental Parameters

The number of co-isolated precursor groups resulting from HRIM-based precursor isolation was compared to the more traditional quadrupole-based approach by performing a meta-analysis of the human proteome. Simulated experiments were defined by several parameters, including throughput, instrument operation mode, and target m/z and/or CCS/z values. Target values were selected to sample the peptide population across the full range of each dimension (Figure 1). The chimeric precursor groups were then extracted by creating a subset of the peptide library containing precursors satisfying the boundary conditions for each pertinent dimension (Figure S1). The bioinformatics analysis and data visualization for the trends in the sizes of chimeric precursor groups were performed in R and Excel.

Throughput conditions were defined by the gradient length and the average full width at half max (FWHM) of the peptide RT peaks as reported in the corresponding application notes by Evosep (Odense, Denmark) [30–35]. The RT boundaries around each target RT were calculated for each throughput condition by dividing the FWHM (in minutes) by the gradient length (in minutes) and then applying the resulting offset symmetrically above and below the target RT. Target RT included the sequence of numbers from 0 to 1 spaced at intervals of 0.05. Peptides with predicted apex RTs that fell within the RT boundaries were considered co-eluting and passed this filtering step.

Target m/z values covering the full range of predicted precursors included the sequence of numbers from 300 to 1800 Th spaced at intervals of 50 Th. Isolation windows of 2 and 20 Th were selected to simulate the isolation during DDA and DIA experiments, respectively. The boundary m/z values for each target m/z and quadrupole isolation window were calculated by dividing the full window width by 2 and applying the offset symmetrically above and below the target m/z.

Target CCS/z values covering the full range of predicted precursors included the sequence of numbers from 100 to 200 Å^2/z spaced at intervals of 10 Å^2/z. The boundary CCS/z values were calculated as similarly described above (see also Figure S1) except with isolation widths of 1% (HRIM) and 5% (low-resolution ion mobility, LRIM) of the separation axis for the SLIM-QTOF and timsTOF systems, respectively. It is important to note that while resolving powers over 1800 for SLIM [36, 37] and up to 300 for TIMS [38, 39] have been demonstrated, these measurements correspond to only narrow regions of the mobility range and much longer acquisition times per mobility separation than what is optimal for LC-based bottom-up proteomics [16, 40]. To best represent the performance and method parameters employed in typical proteomics operation, isolation widths (i.e., peak capacities) and mobility separation time frames were derived directly from empirical data. During proteomics analysis, the typical peak width (FWHM) for a TIMS peak analyzed using a 100 ms TIMS ramp was experimentally measured by Skowronek et al. [41] to be ~5 ms, indicating that each feature corresponds to roughly 5% of the separation axis and the ramp can achieve a peak capacity of 20. The typical FWHM for a SLIM HRIM peak analyzed using a 240 ms SLIM separation time period is ~2 ms, as determined using an automated peak finding algorithm built into Agilent's IM-MS Browser software, indicating that each feature corresponds to roughly 1% of the separation axis corresponding to a peak capacity of 100 [24] (for the mobility range corresponding to doubly charged peptides). Comparative distributions of experimentally measured mobility peak widths for TIMS and SLIM are provided in Figure S2.

2.3 | LC-MS/MS Analysis of HeLa Digest

HeLa digest samples were introduced using an Evosep One system equipped with an EV1107 column at a throughput of 200 samples per day (SPD). A total of 100 ng of HeLa digest was injected per run, and ionization was achieved using an Evosep EV1086 emitter. All data were collected using a modified MOBIE HRIM system (MOBILion Systems, Chadds Ford, PA) coupled to an Agilent 6546 QTOF. For the "Quad only" experiments, the MOBIE system was operated in passthrough mode [26], while the QTOF was run either in targeted MS/MS mode using isolation windows of 1.3 Th or 4 Th, or in data-independent acquisition (DIA) mode with isolation windows of 10 Th or 20 Th. For "IM-only" experiments, the MOBIE system was operated in HRIM mode with the QTOF set to all-ion passthrough (no precursor isolation), and collision energy (CE) was applied to induce fragmentation for fragmentation analysis. For "Quad + IM" experiments, MOBIE was operated in HRIM mode while the quadrupole was configured to isolate precursor ions using predefined isolation windows (1.3 Th, 4 Th, 10 Th, or 20 Th) and apply appropriate CE values.

Quad-only data were analyzed using Agilent MassHunter Qualitative Analysis while IM-only and Quad + IM data were analyzed using Agilent's IM-MS Browser. For IM-only and Quad + IM data, fragmentation spectra were extracted with either a 1% isolation width or a 5% isolation width (Figure S3). Each chromatogram was integrated over the same retention time window before extracting and exporting centroided mass spectra for downstream analysis. Fragmentation spectra for all modes were annotated using the Interactive Peptide Spectral Annotator (IPSA) [42] with consistent settings across acquisition modes. Percent total ion current (% TIC) values were obtained from the summary files exported from each IPSA annotation. Fragmentation spectra were also input into the NIST pep search software to obtain the match probability for peptide sequence identification.

3 | Results

3.1 | Formation of the Peptide Library and Chimeric Precursor Groups

Two pre-trained deep learning models were utilized to create the library of properties for human tryptic peptides. AlphaPeptDeep performed in silico trypsin digestion on the human proteome in addition to prediction of precursor m/z, charge, and RT on the resulting tryptic peptides (Figure 1). DeepCollisionalCrossSection took a list of peptide sequences and their charge states as inputs to predict precursor CCS values (Figure 1). These two libraries of predicted properties were then combined by matching the peptide sequence and precursor z in each library to create a final, fully defined peptide library containing m/z, z, RT, and CCS/z for each sequence.

Chimeric spectra result from precursors that co-elute in the LC dimension and are co-isolated by IM and/or quadrupole filtering during analysis. To simulate the isolation of groups of chimeric precursors, target values in each dimension (i.e., m/z, CCS/z, or RT) that spanned the full range of values in the library served as reference points for each filtering step (Figure 1). In this way, the number of precursors that would be co-isolated (m/z or CCS/z) and co-eluted (RT) was determined by filtering for precursors that had values within a specified window size centered around the target values (Figure S1). For example, in a simulated quadrupole isolation experiment, the peptide library was filtered in the m/z dimension to include only precursors whose m/z values fell within the specified isolation window centered on each target m/z value (e.g., ±10 Th for a 20 Th window) to represent the precursors that would be co-isolated with each theoretical target precursor (Figure 1). This new subset of the peptide library was then filtered in a similar way for the LC dimension, with the co-elution window defined by the FWHM normalized to the corresponding gradient length, as empirically observed with the Evosep LC system [30–35]. Ion mobility experiments were simulated by filtering in the CCS/z and LC dimensions. Finally, the combination of quadrupole and ion mobility isolation was evaluated by filtering in all three dimensions.

Prior to performing the filtering operations, the properties in the peptide library were visualized to assess the accuracy of the deep learning model predictions and better understand the distributions of the peptides across each of the three separation dimensions. The retention times for many of the library peptides were observed to be concentrated at the beginning and end of the gradient, indicating behavior inconsistent with experiments where early and late RT spikes in the total ion chromatogram are not typically observed (Figure 2A). Since most peptide identifications come from the middle of the gradient, the target retention times less than 0.1 and greater than 0.8 were not utilized in the filtering steps so as not to artificially inflate the number of co-isolated precursors. For the percentage of peptide library calculations, the number of co-isolated precursors was divided by 275,298 total precursors, representing the subset of the library containing precursors with RT greater than 0.075 and less than 0.825. The mass and mobility dimensions showed similar asymmetric distributions, with most precursors having m/z values near 450 Th (Figure 2B) and CCS/z near 160 $Å^2/z$ (Figure 2C), accurately reflecting typical experimentally observed distributions. When considering both the mass and mobility dimensions together, two target value combinations with substantially higher density were observed at the lower left corner of the plot, indicating that approximately 9% of the peptide library (i.e., roughly 36,000 precursors) has m/z values between 400 and 450 Th and CCS/z values between 150 and 160 $Å^2/z$, while approximately 8.5% of the library has m/z values between 450 and 500 Th and CCS/z between 160 and 170 $Å^2/z$. In addition, the predicted precursors formed charge-dependent trendlines that are very similar to those observed in experimental ion mobility-mass spectrometry data (Figure 2E). Plotting the precursor m/z and CCS/z values also revealed that precursors with low m/z and CCS/z values tend to have very short retention times, while precursors with higher values tend to have longer retention times (Figure 2F). This trend seems to indicate a relationship between the vertical position of ions within a given charge state trend line and the polarity of the molecular structure, with more polar peptides having more compact gas phase structures and more nonpolar peptides having more extended gas phase structures. For each precursor charge state, there was also a positive correlation between precursor CCS/z and retention time, further highlighting the relation between peptide polarity and gas phase structure (compare Figure 2E,F).

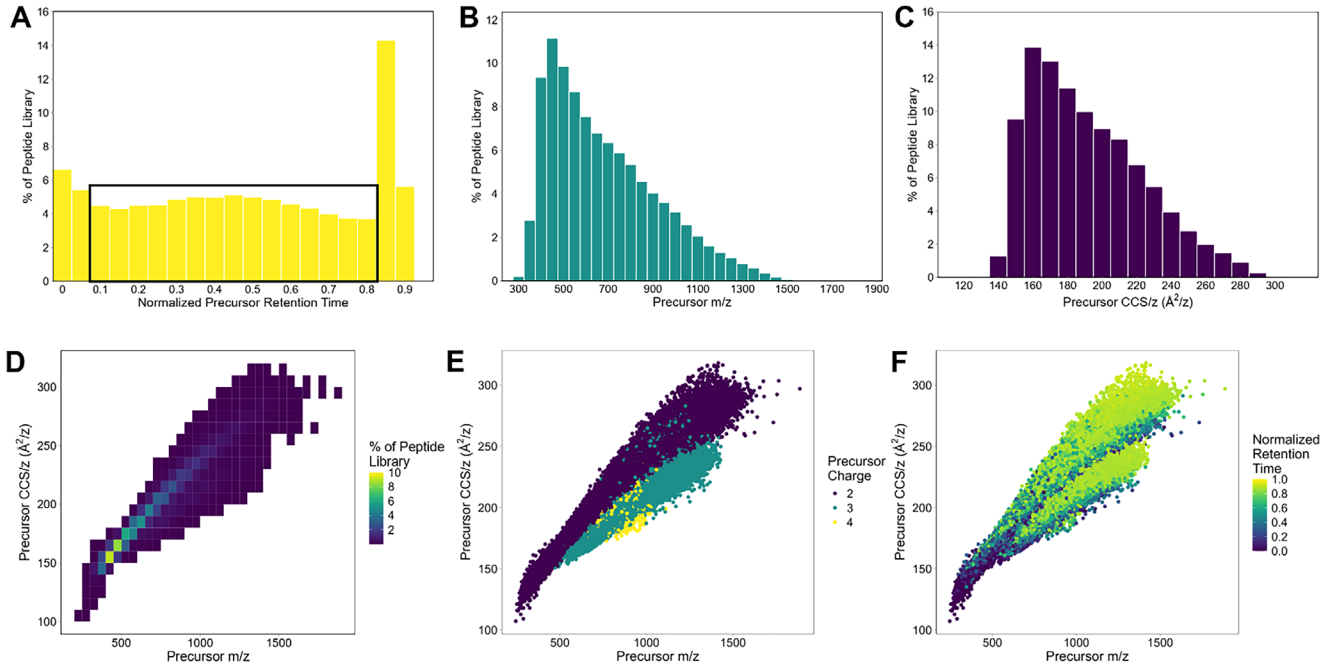

FIGURE 2 | Distribution of precursor properties in the in-silico peptide library. Panels A–C are histograms showing the percentage of the peptide library covered as a function of (A) normalized precursor RT (bin width = 0.05), (B) precursor *m/z* (bin width = 50 Th, bins centered at target *m/z* values), and (C) precursor CCS/z (bin width = 10 Å^2/z). Panels D–F depict two-dimensional distributions of precursor CCS/z versus precursor *m/z*; (D) density map colored by the percentage of the peptide library per bin, (E) data colored by precursor charge state (z), and (F) data colored by normalized retention time.

3.2 | Analysis of Chimeric Precursor Groups

Chimeric precursor groups defined by their respective target values were evaluated for their size at various isolation widths for the three isolation approaches. Scatter plots of the precursor CCS/z against the precursor *m/z* revealed the expected patterns for precursors (Figure 3A–C, white dots) included in each type of chimeric group. For instance, the 10 Th quadrupole isolation window (Figure 3A) formed vertical strips of precursors centered around each target precursor *m/z* value. Combining ion mobility isolation with quadrupole isolation formed rectangular groupings due to filtering in both the *m/z* and CCS/z dimensions (Figure 3B). In contrast to quadrupole isolation, the 1% ion mobility isolation windows formed horizontal strips of precursors centered around the target CCS/z values. The size of the quadrupole-induced chimeric precursor groups peaked at *m/z* 450 for the 10 Th window, which reflects the densest region of the *m/z* dimension (Figure 2B). Even with a wider quadrupole isolation width of 25 Th, adding additional isolation with the 1% ion mobility isolation width decreased the maximum size of the chimeric precursor groups by ~4x (Figure 3B). The size of the ion mobility-induced chimeric precursor groups peaked at CCS/z 170 Å^2/z, reflecting the densest region of the CCS/z dimension (Figure 2C). For each of the instrument modes, the sizes of the chimeric precursor groups were also analyzed by target retention time. There tended to be larger chimeric groups in the first half of the gradient, especially near the peak *m/z* (Figure 3D,E) and CCS/z values (Figure 3F). In addition, the largest chimeric precursor group formed by HRIM 1% isolation (Figure 3F) was smaller than that formed by quadrupole isolation with a 10 Th window (Figure 3D). Overall, combining quadrupole (25 Th) and HRIM (1%) isolation (Figure 3E) produced smaller chimeric precursor groups than either isolation mode alone. The isolation in both *m/z* and CCS/z dimensions attained by combining quadrupole and HRIM isolation modes is evident in the corresponding contour plot (Figure 3E) compared to that of quadrupole isolation (Figure 3D) or mobility isolation (Figure 3F) alone. In addition, the size of chimeric precursor groups resulting from representative DDA or DIA conditions with quadrupole isolation were examined as a function of the target *m/z* values (Figure 3G,H) and with ion mobility isolation as a function of the target CCS/z values (Figure 3I). As expected, the size of the chimeric precursor group reaches a maximum at the densest region of the respective mass and mobility dimensions (Figures 3G–I and S4). Interestingly, the HRIM method (1% isolation width) (Figure 3I), which is inherently data-independent on SLIM-based instruments (since ions over the full mobility range are isolated in each scan), produces smaller chimeric precursor groups than the 20 Th window often used for DIA experiments on quadrupole-based instruments (Figure 3G). Notably, performing a DDA-like quadrupole + HRIM experiment with a 2 Th window at 1% HRIM isolation width (Figure 3H, green circles) greatly decreases the chimeric precursor group size relative to a QTOF-based DDA experiment (Figure 3G, circles), whereas performing a similar experiment at the 5% isolation width (Figure 3H, blue circles) representative of a TIMS-based instrument only moderately decreases the chimeric group size. Relative to a 2 amu quadrupole isolation window alone, adding 1% HRIM isolation width to quadrupole isolation resulted in a 13× decrease in chimeric precursor group size whereas adding 5% LRIM isolation width only resulted in a 2× decrease on average across all target *m/z*'s investigated.

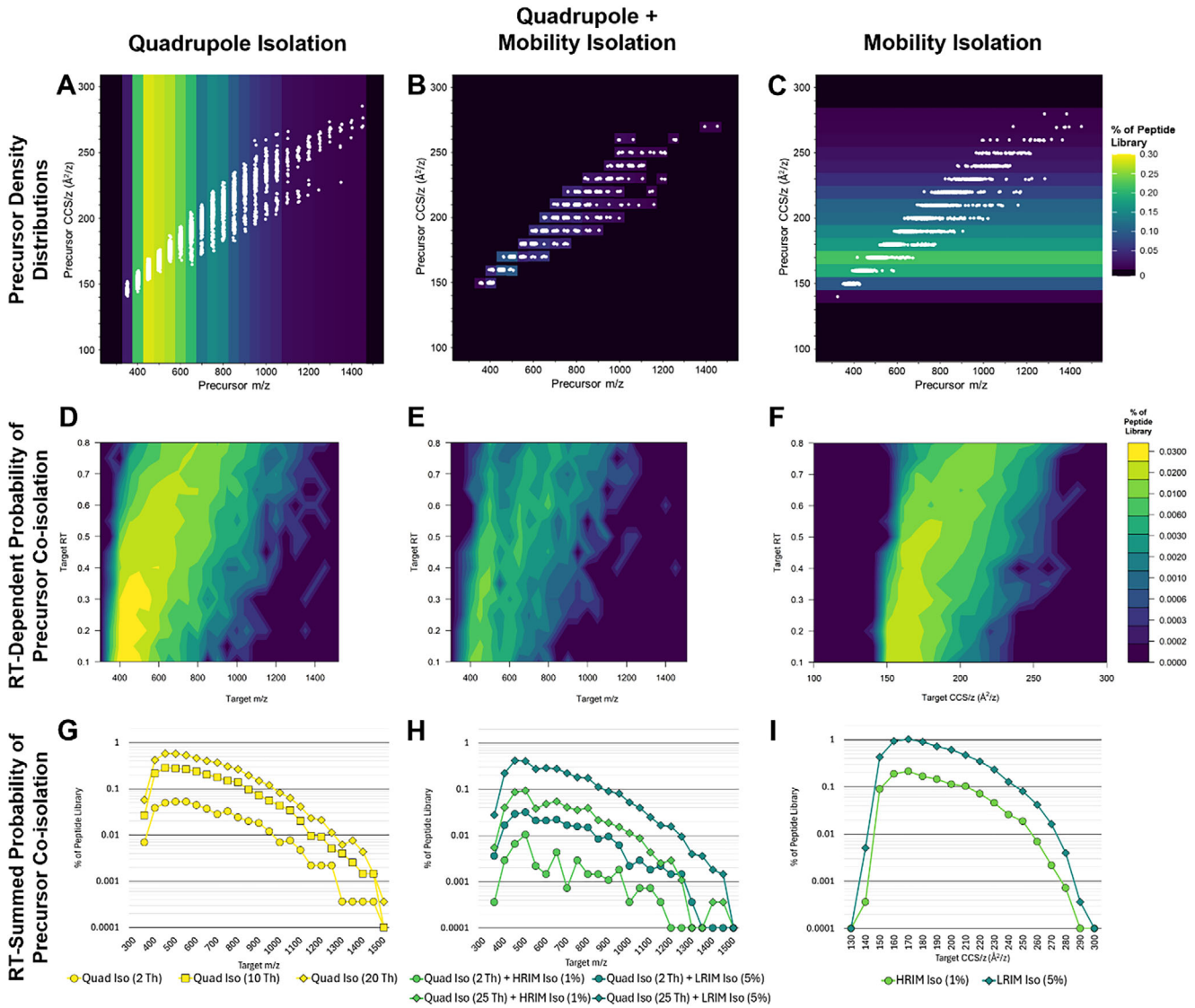

FIGURE 3 | Simulated chimeric frequency across different instrument modes. Panels A–C are precursor selection maps showing the number of precursors transmitted per isolation window across different isolation methods, all assuming a throughput of 200 samples per day (SPD): (A) quadrupole-only isolation with 10 Th windows, (B) combined quadrupole (25 Th) + HRIM (1% CCS/z isolation width), and (C) HRIM-only isolation with 1% CCS/z width. The color scale represents the total number of precursors per isolation bin. Panels D–F are heatmaps depicting the percentage of the peptide library transmitted at each target *m/z* (D, E) or CCS/z (E, F) and RT for the same modes as in A–C, respectively. Panels G–I are line plots summarizing the percentage of the peptide library detected as a function of target *m/z* (G, H) or CCS/z (H, I), for the same modes as in A–C, respectively. Panel G shows quadrupole-only isolation using 2, 10, and 20 Th isolation windows. Panel H presents results for quadrupole + IM isolation, using isolation windows of 2 Th + 1% CCS/z, 2 Th + 5% CCS/z, 25 Th + 1% CCS/z, and 25 Th + 5% CCS/z, respectively. Panel I displays the results for IM-only isolation using 1% and 5% CCS/z isolation windows.

The effect of throughput on the size of chimeric precursor groups was also examined for each instrument mode. Regardless of the instrument mode, higher throughputs resulted in larger chimeric groups (Figures 4 and S4). The higher chromatographic resolution attained at lower throughputs and longer LC gradients thus decreases the number of co-eluted and co-isolated precursors because there is sufficient separation between precursor retention times in the LC dimension. In addition, chimeric precursor groups at the most concentrated regions were larger across all throughputs than those at less concentrated regions for quadrupole-only isolation (Figure 4A vs. D), HRIM-only isolation with 1% width (Figure 4B vs. E), and LRIM-only isolation with 5% width (Figure 4C vs. F). At the densest region, defined by *m/z* 450 for quadrupole isolation and CCS/z 170 Å^2/z for ion mobility, isolating precursors with a 1% ion mobility isolation width is comparable to a 10 Th quadrupole window (Figure 4A vs. B). At a sparser region, defined by *m/z* 1000 for quadrupole isolation and CCS/z 250 Å^2/z for ion mobility, isolating precursors with a 1% ion mobility isolation width is equivalent to a 5 Th quadrupole window (Figure 4D vs. E). The 5% ion mobility isolation width attained with TIMS-based instruments generates chimeric precursor groups larger than those of a 20 Th quadrupole window (Figure 4A vs. C and 4D vs. F).

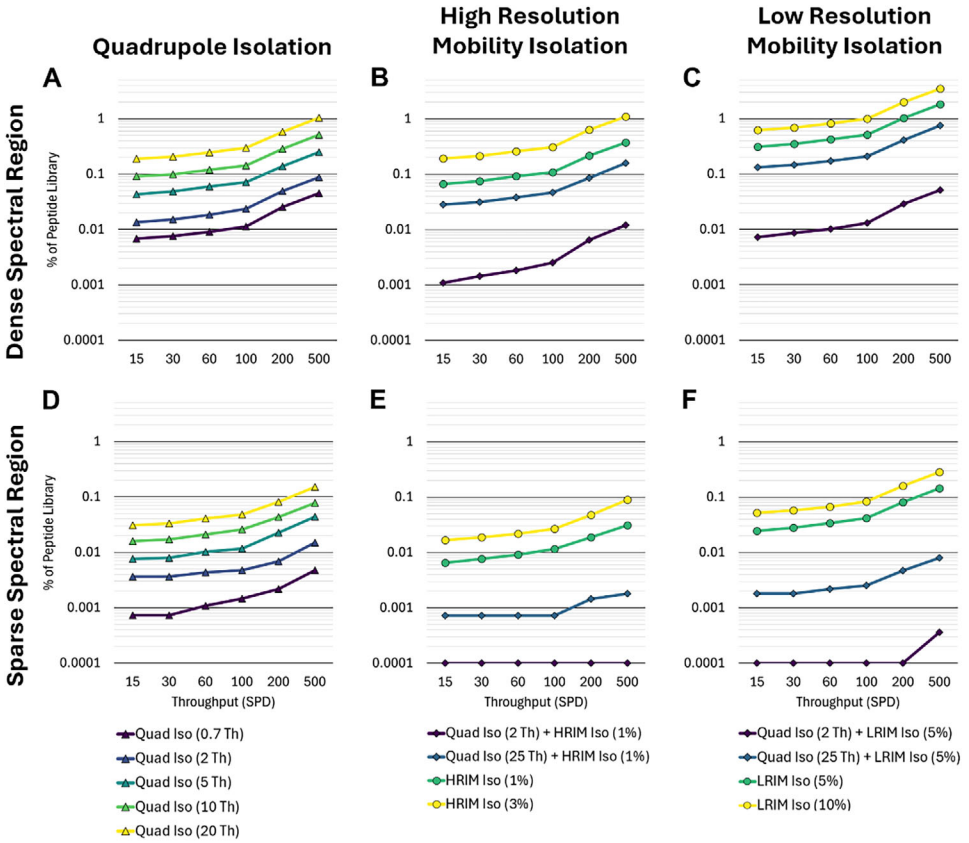

FIGURE 4 | Effect of throughput on the rate of chimeric spectra across different instrument modes at various target m/z and CCS/z values. The percentage of the peptide library captured is plotted as a function of throughput for various instrument modes representing dense and sparse target values. Throughputs of 15, 30, 60, 100, 200, and 500 SPD correspond to chromatographic gradients of 88, 44, 21, 11.5, 5.6, and 2.2 min, respectively. (A, D) Quadrupole-only results are shown for target m/z values of 450 Th (A) and 1000 Th (D), using isolation window widths of 0.7, 2, 5, 10, and 20 Th. (B, E) HRIM-only and quadrupole + HRIM results are shown for target CCS/z values of 170 Å^2 (B) and 250 Å^2 (E). For quadrupole + HRIM, the corresponding target m/z values are 450 Th (B) and 1000 Th (E), with quadrupole window widths of 2 or 25 Th combined with HRIM windows of 1% or 3% relative width in CCS/z space. (C, F) LRIM-only and quadrupole + LRIM co-isolation results are shown at CCS/z targets of 170 Å^2 (C) and 250 Å^2 (F), using LRIM windows of 5% or 10% relative width in CCS/z space. For quadrupole + LRIM in panels (C) and (F), quadrupole window widths of 2 or 25 Th were combined with LRIM windows of 5% or 10% relative width, at target m/z values of 450 Th (C) and 1000 Th (F). Across all panels, the y-axis is plotted on a logarithmic scale to illustrate the dynamic range of precursor coverage.

3.3 | Effect of Instrument Mode on Chimeric Overlap of Experimental Spectra

To empirically assess the selectivity of precursor isolation across various quadrupole and IM settings, 100 ng of HeLa digest was analyzed in three different instrument modes (quadrupole-only, quadrupole and IM, or IM-only isolation) on the same system using the same LC method. For each instrument mode, respective MS1 spectra (Figure S5), MS/MS spectra, ion chromatograms, and ion mobilograms were extracted for a low abundance peptide with the sequence "DFMIQGGDFTR" (precursor m/z 643.7953), representative of the dense region of the precursor m/z range. To estimate the specificity of the fragmentation spectra across instrument modes, we compared the percent total ion current explained (% TIC Explained), defined as the percentage of the total ion current of the fragmentation spectrum that can be explained by matched fragment ions. As expected, there was a lower percentage of the total ion current associated with the target peptide sequence when spectra were acquired with a wide 20 Th quadrupole isolation window (Figure 5A) typically used for DIA experiments, compared to that when spectra were acquired with the narrow 1.3 Th isolation window (Figure 5B) typically used for DDA experiments. Quadrupole-only isolation with the 20 Th window resulted in very low relative abundance peptide fragment ions (Figure 5C), demonstrating a high degree of chimeric content within the MS/MS spectrum and lack of selectivity in precursor isolation, which was also observed at the MS1 level (Figure S5). Manual annotation of the characteristic peptide fragment ions confirms the target peptide's presence, but the low quality of the signals within the abundant chimeric background is anticipated to preclude automated detection using typical search programs. However, combining the 20 Th quadrupole isolation window with IM significantly reduces the complexity of the spectra (Figures 5A and S5), which is reflected in the lower number of background peaks when the spectra were extracted with a 5% LRIM isolation width, simulating the resolution attained with a timsTOF instrument (Figure 5E), or a 1% HRIM isolation width, representing the resolution attained with a SLIM-QTOF instrument (Figure 5G). In fact, operating the SLIM-QTOF (HRIM 1%) with a 20 Th window showed comparable specificity to utilizing quadrupole only isolation with a 1.3 Th window for this target peptide (Figure 5A vs. B). Operating the SLIM-QTOF

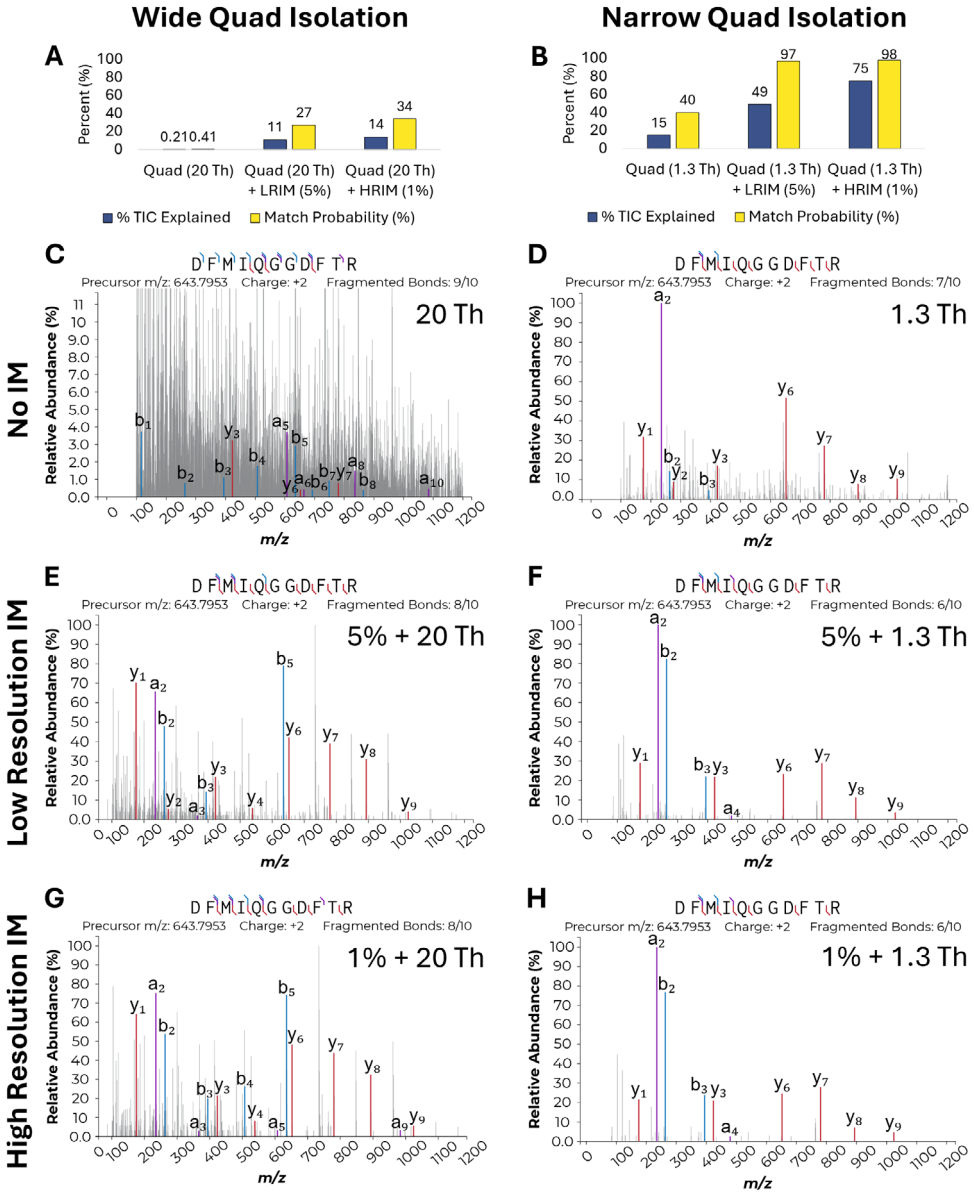

FIGURE 5 | Example spectra demonstrating various levels of chimeric overlap observed with different instrument modes for precursor isolation. Panels (A) and (B) quantify for spectra in panels (C–H) how much intensity the target peptide's fragment ions contribute to the total ion current and the NIST % Match Probability for the fragment spectrum to a library spectrum for the DFMIQGGDFTR peptide. Panels (C) and (D) show annotated spectra acquired with quadrupole isolation with a 20 Th window (C) and a 1.3 Th window (D). Panels (E) and (F) show annotated spectra extracted with a 5% LRIM isolation width combined with quadrupole isolation with a 20 Th window (E) and a 1.3 Th window (F). Panels (G) and (H) show annotated spectra extracted with a 1% HRIM isolation width combined with quadrupole isolation using a 20 Th window (G) and a 1.3 Th window (H).

with HRIM isolation alone produced specificity greater than the 4 Th window and less than the 1.3 Th window for this target peptide (Figure S6), which is better than the predicted specificity (Figure 4). In both cases, the ability to achieve improved specificity while leveraging wider or no quad isolation can be translated experimentally into greater sensitivity, analysis range, and/or LC acquisition rate since the need for narrow quadrupole filtering typically limits performance in each of these aspects. Combining quadrupole isolation with a 1.3 Th window and 1% HRIM isolation further increased the purity of the spectrum (Figure 5B). Spectra acquired with a combination of quadrupole and IM isolation contain significantly less background signal (Figure 5F,H). Ultimately, the highest specificity was obtained when employing a combination of narrow quadrupole and HRIM precursor isolation (Figure 5H), which could facilitate peptide identification, PTM site localization, and de novo sequencing in cases of high chimeric overlap.

4 | Discussion

The goal of proteomics is to identify and quantify proteins in biological samples. This process is facilitated by finding precursors that are fragmented to provide information about their peptide sequences, leading to association with their protein identities. Ideally, one precursor would be fragmented per MS2 spectrum to ensure successful identification of the corresponding peptide sequence. However, due to the large

number of proteins in more complex samples, such as cell lysates or tissues, hundreds of precursors can have the same retention time and very similar *m/z* values. Co-isolation of these peptides with similar properties results in chimeric spectra that contain fragment ions from all the present peptides, thus complicating peptide sequence identification. In tandem with computational methods to help identify the additional peptides present in chimeric spectra, increasing the selectivity of analysis using different modes of instrument operation, such as HRIM, decreases the likelihood of generating chimeric spectra in the first place.

To better understand the likelihood of precursor co-isolation during different modes of instrument operation, a library of peptides and their properties was leveraged as a model for theoretical analysis. To simplify our model, all peptides in the library were assumed to be equally abundant and no modifications, including standard ones like oxidation or carbamidomethylation, were considered. This library of precursors provides a representative population that approximates the typical level of experimental complexity encountered enabling relative comparisons between the various precursor isolation techniques explored. Co-isolation of precursors was simulated by filtering precursor values using thresholds defined by each mode of instrument operation. Comparing the corresponding sizes of the groups of co-isolated precursors provides a relative quantification of specificity for each operation mode and these trends can then enable a mapping of SLIM-QTOF operation modes to specific proteomics workflows based on where current methods with equivalent specificity have demonstrated success, as summarized in Table 1. For example, timsTOF systems generate data equivalent to the combined operating modes of ion mobility with 5% LRIM isolation widths and quadrupole-isolation, most often with 20–25 Th windows or 2–3 Th windows depending on the desired level of specificity. The SLIM-QTOF instrument is equivalent to the ion mobility operating mode with 1% HRIM isolation widths.

Quadrupole-based isolation provides separation in the mass dimension, with wider isolation windows (10–20 Th) often used for data-independent acquisition. While the wider windows devote more instrument time to a larger range of precursors, the limited specificity of the resulting MS2 spectra can complicate peptide sequence identification. Narrow isolation windows (<2 Th) are utilized for DDA. Limiting the number of precursors in each MS2 spectrum increases the specificity of analysis, but narrow quadrupole windows come at the cost of ion utilization since less time can be spent analyzing each window while maintaining a certain LC acquisition rate (MS1/MS2 cycle time). Ultimately, quadrupole-based isolation for DIA mode with wider isolation windows works best for high throughput assays [43, 44], quantifying differential expression [45, 46], deep proteome coverage [44], and single cell proteomics [47] because it maximizes sensitivity, LC acquisition rate, and mass analysis range. Quadrupole-based isolation for DDA mode with narrow isolation windows is often applied to analysis of PTMs [48–50], peptide cross-linking [51, 52], immunopeptidomics [53], and biofluids [49, 54, 55] where clean MS2 spectra for confident identification is prioritized over other metrics.

Ion mobility-based isolation provides separation in the mobility dimension, which is dependent on the size, shape, and charge of precursors rather than *m/z*. High resolution ion mobility with 1% isolation widths was theoretically predicted to fall between the specificities of a 5 Th and 10 Th quadrupole window (Figures 3 and 4) and experimentally observed to fall between a 1.3 Th and 4 Th quadrupole window (Figure S6). In addition, HRIM at 1% isolation offers the advantages of (1) significantly higher (near 100%) ion utilization since ions are temporally separated and all transmitted rather than sequentially filtered, allowing for enhanced sensitivity, (2) higher rates of MS2 spectral generation (>500 Hz) owing to the narrow mobility peaks (~2 ms), (3) full range of analysis so that peptides across the full *m/z* range are detectable, and 4) generation of separate MS2 spectra for isomeric and isobaric peptides that are mobility resolved. HRIM-only isolation is anticipated to offer particular advantages in performance for single cell and sample limited analyses based on the substantial increase in ion sampling achieved relative to Quad-only isolation (~100% vs. 0.5%–2%) [7, 56].

The combination of quadrupole and ion mobility isolation provides unparalleled specificity due to separation occurring in both the mass and mobility dimensions. The decrease in ion utilization for combined quadrupole and ion mobility isolation is compensated by the increased coverage of diverse precursors and specificity of the MS2 spectra. Applying a wide or narrow quadrupole isolation window to HRIM at 1% isolation width can approximately triple the specificity compared to ion mobility isolation alone (Figure 5). Experimentally, we showed that adding HRIM isolation at 1% widths to a 25 Th quadrupole isolation window has spectral specificity between a 1.3 Th and a 4 Th quadrupole window, indicating a possibly 10-fold reduction in complexity of the *m/z* dimension. This almost 10-fold reduction is more than double the 4-fold reduction observed using a timsTOF instrument [23].

Increasing spectral specificity while maintaining sufficient ion utilization is powerful for facilitating peptide sequence identification in complex samples. The combination of IM and quad isolation with wide windows in DIA mode works well for high throughput assays [57–59], quantifying differential expression [60], deep proteome coverage [61], single cell proteomics [60, 62], PTM analysis [63, 64], and peptide cross-linking [65, 66]. IM and quad isolation with narrow windows in DDA mode works well for PTM analysis [67–69], peptide cross-linking [70], immunopeptidomics [71–73], and analyzing biofluids [73, 74].

5 | Concluding Remarks

The theoretical and experimental analysis performed for the various isolation approaches provides a foundation for comparing their specificity of analysis and projecting application areas where each mode would be best leveraged. HRIM isolation alone on a SLIM-QTOF instrument was found to be comparable to a ~5 Th quadrupole isolation window and to produce smaller chimeric precursor groups than those predicted from a timsTOF instrument. Increasing ion mobility resolution was verified to increase specificity in precursor isolation and is anticipated to enhance the speed, depth, and coverage achievable in proteomics workflows when coupled with a high performance QTOF platform. The utility of ion mobility to increase the efficiency of ion sampling as well as speed and specificity for MS2 generation as

TABLE 1 | Summary of characteristics for quadrupole isolation, HRIM isolation, and the combination of quadrupole and IM isolation.

Instrument mode	Isolation width	Specificity	Ion utilization	Suitable proteomic workflows
Quadrupole only	DIA (2-20 Th)			• High throughput • Differential expression • Deep proteome coverage • Single cell proteomics
	DDA (0.7-4 Th)			• PTMs • Peptide cross-linking • Immuno-peptidomics • Biofluids
HRIM	1%			• High throughput • Differential expression • Single cell proteomics
IM + Quad	DIA (5-40 Th)			• High throughput • Differential expression • Deep proteome coverage • Single cell proteomics • PTMs • Peptide cross-linking
	DDA (0.7-4 Th)			• PTMs • Peptide cross-linking • Immuno-peptidomics • Biofluids

demonstrated on timsTOF instruments can be further extended by leveraging higher resolution ion mobility technologies like SLIM. We therefore predict that high resolution ion mobility will play a growing role in maximizing performance for future generations of proteomics instrumentation.

Author Contributions

I.R.U. performed all peptide library meta-analysis and lead drafting of the manuscript. L.D. performed experimental data collection and analysis. M.F., L.R. III, L.R., and D.D. provided experimental design and data review input. The manuscript was written through contributions of all authors and all authors have given approval to the final version of the manuscript.

Acknowledgments

The authors would like to thank Alexey Nesvizhskii and Ben Orsburn for discussions and recommendations during the preparation of this study.

Funding

The authors have nothing to report.

Conflicts of Interest

All authors are employees of MOBILion Systems, Inc. The authors declare no other competing financial interest.

Data Availability Statement

Mass spectrometry raw files are accessible on the MassIVE database under accession code MSV000098195.

References

1. R. Aebersold and M. Mann, "Mass-Spectrometric Exploration of Proteome Structure and Function," *Nature* 537 (2016): 347–355, https://doi.org/10.1038/nature19949.

2. N. P. Manes and A. Nita-Lazar, "Application of Targeted Mass Spectrometry in Bottom-Up Proteomics for Systems Biology Research," *Journal of Proteomics* 189 (2018): 75–90, https://doi.org/10.1016/j.jprot.2018.02.008.

3. C. S. Movassaghi, J. Sun, Y. Jiang, et al., "Recent Advances in Mass Spectrometry-Based Bottom-Up Proteomics," *Analytical Chemistry* 97 (2025): 4728–4749, https://doi.org/10.1021/acs.analchem.4c06750.

4. S. Houel, R. Abernathy, K. Renganathan, K. Meyer-Arendt, N. G. Ahn, and W. M. Old, "Quantifying the Impact of Chimera MS/MS Spectra on Peptide Identification in Large-Scale Proteomics Studies," *Journal of Proteome Research* 9 (2010): 4152–4160, https://doi.org/10.1021/pr1003856.

5. W. Zhang, Z. Liang, X. Chen, et al., "ChimST: An Efficient Spectral Library Search Tool for Peptide Identification From Chimeric Spectra in Data-Dependent Acquisition," *IEEE/ACM Transactions on Computational Biology and Bioinformatics* 18, no. 4 (2021): 1416–1425, https://doi.org/10.1109/TCBB.2019.2945954.

6. P. H. Dawson, *Quadrupole Mass Spectrometry and Its Applications* (Elsevier Science, 1976).

7. D. DeBord, L. C. Rorrer, L. Deng, and F. G. Strathmann, "Abandoning the Quadrupole for Mass Spectrometry Fragmentation Analysis: Towards 1,000 Hz Speeds With 100% Ion Utilization Using High Resolution Ion Mobility Precursor Isolation," bioRxiv 2024.10.18.619158 (2024), https://doi.org/10.1101/2024.10.18.619158.

8. V. Dorfer, S. Maltsev, S. Winkler, and K. Mechtler, "CharmeRT: Boosting Peptide Identifications by Chimeric Spectra Identification and Retention Time Prediction," *Journal of Proteome Research* 17 (2018): 2581–2589, https://doi.org/10.1021/acs.jproteome.7b00836.

9. R. Lou and W. Shui, "Acquisition and Analysis of DIA-Based Proteomic Data: A Comprehensive Survey in 2023," *Molecular & Cellular Proteomics* 23 (2024): 100712, https://doi.org/10.1016/j.mcpro.2024.100712.

10. D. Shteynberg, L. Mendoza, M. R. Hoopmann, et al., "reSpect: Software for Identification of High and Low Abundance Ion Species in Chimeric Tandem Mass Spectra," *Journal of the American Society for Mass Spectrometry* 26 (2015): 1837–1847, https://doi.org/10.1007/s13361-015-1252-5.

11. B. Zhang, M. Pirmoradian, A. Chernobrovkin, and R. A. Zubarev, "DeMix Workflow for Efficient Identification of Cofragmented Peptides in High Resolution Data-Dependent Tandem Mass Spectrometry," *Molecular & Cellular Proteomics* 13 (2014): 3211–3223, https://doi.org/10.1074/mcp.O114.038877.

12. M. Frejno, M. T. Berger, J. Tüshaus, et al., "Unifying the Analysis of Bottom-Up Proteomics Data With CHIMERYS," *Nat Methods* 22 (2025): 1017–1027, https://doi.org/10.1038/s41592-025-02663-w.

13. F. Meier, A.-D. Brunner, M. Frank, et al., "diaPASEF: Parallel Accumulation–Serial Fragmentation Combined With Data-Independent Acquisition," *Nature Methods* 17 (2020): 1229–1236, https://doi.org/10.1038/s41592-020-00998-0.

14. H. Chi, C. Liu, H. Yang, et al., "Comprehensive Identification of Peptides in Tandem Mass Spectra Using an Efficient Open Search Engine," *Nature Biotechnology* 36 (2018): 1059–1061, https://doi.org/10.1038/nbt.4236.

15. C. S. Hoaglund-Hyzer, J. Li, and D. E. Clemmer, "Mobility Labeling for Parallel CID of Ion Mixtures," *Analytical Chemistry* 72 (2000): 2737–2740, https://doi.org/10.1021/ac0000170.

16. J. A. Mclean, B. T. Ruotolo, K. J. Gillig, and D. H. Russell, "Ion Mobility–Mass Spectrometry: A New Paradigm for Proteomics," *International Journal of Mass Spectrometry* 240 (2005): 301–315, https://doi.org/10.1016/j.ijms.2004.10.003.

17. D. Cooper-Shepherd, "Comprehensive Biotherapeutic Characterization Enabled by Electron Capture Dissociation on the SELECT SERIES™ Cyclic™ IMS Mass Spectrometer," Waters Application Note, 720008287 (2025), https://www.waters.com/content/dam/waters/en/app-notes/2024/720008287/720008287-en.pdf.

18. M. Daly, "Cyclic™ Ion Mobility Unravels Sites of Chemically Induced Deamidation," Waters Application Note, 720008215 (2024), https://www.waters.com/content/dam/waters/en/app-notes/2024/720008215/720008215-en.pdf.

19. S. Ippoliti, "Confident O-Glycosylation Site Identification for ENBREL (etanercept) Using the ECD Functionality of SELECT SERIES Cyclic IMS System," Waters Application Note, 720007458 (2021), https://www.waters.com/content/dam/waters/en/app-notes/2021/720007458/720007458-en.pdf.

20. L. Morrison, "Comprehending COVID-19: Structural Characterization of the Glycan Assemblies of O-Linked Glycopeptides Using Cyclic Ion Mobility," Waters Application Note 720007081 (2021), https://www.waters.com/content/dam/waters/en/app-notes/2021/720007081/720007081-en.pdf.

21. R. S. Glaskin, "Examining the Structural Influence of Site-Specific Phosphorylation by Ion Mobility Mass Spectrometry," Agilent Application Note 5994-1617EN (2019), https://www.agilent.com/cs/library/applications/application-phosphorylation-ims-6560-im-lc-q-tof-5994-1617en-agilent.pdf?srsltid=AfmBOopibSLwXYwrIBoVkOzZtuXd-b5FKbbh97BWJzYeKDjdSROjJb1S.

22. S. E. Haynes, D. A. Polasky, S. M. Dixit, et al., "Variable-Velocity Traveling-Wave Ion Mobility Separation Enhancing Peak Capacity for Data-Independent Acquisition Proteomics," *Analytical Chemistry* 89 (2017): 5669–5672, https://doi.org/10.1021/acs.analchem.7b00112.

23. J. Charkow and H. L. Röst, "Trapped Ion Mobility Spectrometry Reduces Spectral Complexity in Mass Spectrometry-Based Proteomics," *Analytical Chemistry* 93 (2021): 16751–16758, https://doi.org/10.1021/acs.analchem.1c01399.

24. L. Rorrer, J. Srock, R. Kurulugama, M. Fico, and D. DeBord, "Tailoring Separations in SLIM With Traveling Wave Gradients," 319554, Thursday, in *Proceedings of the 72nd ASMS Conference on Mass Spectrometry and Allied Topics*, June 2-6, 2024 (2024).

25. L. Deng, Y. M. Ibrahim, A. M. Hamid, et al., "Ultra-High Resolution Ion Mobility Separations Utilizing Traveling Waves in a 13 M Serpentine Path Length Structures for Lossless Ion Manipulations Module," *Analytical Chemistry* 88, no. 18 (2016): 8957–8964, https://doi.org/10.1021/acs.analchem.6b01915.

26. J. R. Arndt, K. L. Wormwood Moser, G. Van Aken, et al., "High-Resolution Ion-Mobility-Enabled Peptide Mapping for High-Throughput Critical Quality Attribute Monitoring," *Journal of the American Society for Mass Spectrometry* 32 (2021): 2019–2032, https://doi.org/10.1021/jasms.0c00434.

27. A. M. Hamid, S. V. B. Garimella, Y. M. Ibrahim, et al., "Achieving High Resolution Ion Mobility Separations Using Traveling Waves in Compact Multiturn Structures for Lossless Ion Manipulations," *Analytical Chemistry* 88 (2016): 8949–8956, https://doi.org/10.1021/acs.analchem.6b01914.

28. W.-F. Zeng, X. X. Zhou, S. Willems, et al., "AlphaPeptDeep: A Modular Deep Learning Framework to Predict Peptide Properties for Proteomics," *Nature Communications* 13 (2022): 7238, https://doi.org/10.1038/s41467-022-34904-3.

29. F. Meier, N. D. Köhler, A.-D. Brunner, et al., "Deep Learning the Collisional Cross Sections of the Peptide Universe From a Million Experimental Values," *Nature Communications* 12 (2021): 1185, https://doi.org/10.1038/s41467-021-21352-8.

30. https://www.evosep.com/evosep-one-methods/standard-methods/200-spd/.

31. https://www.evosep.com/evosep-one-methods/standard-methods/100-spd/.

32. https://www.evosep.com/evosep-one-methods/standard-methods/60-spd/.

33. https://www.evosep.com/evosep-one-methods/standard-methods/30-spd/.

34. Evosep Application Note AN-012B.

35. https://www.evosep.com/evosep-one-methods/standard-methods/500-spd/.

36. L. Deng, I. K. Webb, S. V. B. Garimella, et al., "Serpentine Ultralong Path With Extended Routing (SUPER) High Resolution Traveling Wave Ion Mobility-MS Using Structures for Lossless Ion Manipulations," *Analytical Chemistry* 89, no. 8 (2017): 4628–4634, https://doi.org/10.1021/acs.analchem.7b00185.

37. J. C. May, K. L. Leaptrot, B. S. Rose, et al., "Resolving Power and Collision Cross Section Measurement Accuracy of a Prototype High-Resolution Ion Mobility Platform Incorporating Structures for Lossless

Ion Manipulation," *Journal of the American Society for Mass Spectrometry* 32 (2021): 1126–1137, https://doi.org/10.1021/jasms.1c00056.

38. M. E. Ridgeway, J. A. Silveira, J. E. Meier, and M. A. Park, "Microheterogeneity Within Conformational States of Ubiquitin Revealed by High Resolution Trapped Ion Mobility Spectrometry," *Analyst* 140 (2015): 6964–6972, https://doi.org/10.1039/C5AN00841G.

39. J. A. Silveira, M. E. Ridgeway, and M. A. Park, "High Resolution Trapped Ion Mobility Spectrometery of Peptides," *Analytical Chemistry* 86 (2014): 5624–5627, https://doi.org/10.1021/ac501261h.

40. F. Meier, M. A. Park, and M. Mann, "Trapped Ion Mobility Spectrometry and Parallel Accumulation–Serial Fragmentation in Proteomics," *Molecular & Cellular Proteomics* 20 (2021): 100138, https://doi.org/10.1016/j.mcpro.2021.100138.

41. P. Skowronek, F. Krohs, M. Lubeck, et al., "Synchro-PASEF Allows Precursor-Specific Fragment Ion Extraction and Interference Removal in Data-Independent Acquisition," *Molecular & Cellular Proteomics* 22 (2023): 100489, https://doi.org/10.1016/j.mcpro.2022.100489.

42. D. R. Brademan, N. M. Riley, N. W. Kwiecien, and J. J. Coon, "Interactive Peptide Spectral Annotator: A Versatile Web-Based Tool for Proteomic Applications," *Molecular & Cellular Proteomics* 18 (2019): S193–S201, https://doi.org/10.1074/mcp.TIR118.001209.

43. A. H. Kverneland, F. Harking, J. M. Vej-Nielsen, et al., "Fully Automated Workflow for Integrated Sample Digestion and Evotip Loading Enabling High-Throughput Clinical Proteomics," *Molecular & Cellular Proteomics* 23 (2024): 100790, https://doi.org/10.1016/j.mcpro.2024.100790.

44. L. R. Serrano, T. M. Peters-Clarke, T. N. Arrey, et al., "The One Hour Human Proteome," *Molecular & Cellular Proteomics* 23 (2024): 100760, https://doi.org/10.1016/j.mcpro.2024.100760.

45. J. Ma, M. Liu, Y. Wang, et al., "Quantitative Proteomics Analysis of Young and Elderly Skin With DIA Mass Spectrometry Reveals New Skin Aging-Related Proteins," *Aging* 12 (2020): 13529–13554, https://doi.org/10.18632/aging.103461.

46. S. Sidoli, R. Fujiwara, and B. A. Garcia, "Multiplexed Data Independent Acquisition (MSX-DIA) Applied by High Resolution Mass Spectrometry Improves Quantification Quality for the Analysis of Histone Peptides," *Proteomics* 16 (2016): 2095–2105, https://doi.org/10.1002/pmic.201500527.

47. Y. Wang, T.-S. M. Lih, L. Chen, et al., "Optimized Data-Independent Acquisition Approach for Proteomic Analysis at Single-Cell Level," *Clinical Proteomics* 19 (2022): 24, https://doi.org/10.1186/s12014-022-09359-9.

48. J. C. L. Maliepaard, J. M. A. Damen, G.-J. P. H. Boons, and K. R. Reiding, "Glycoproteomics-Compatible MS/MS-Based Quantification of Glycopeptide Isomers," *Analytical Chemistry* 95 (2023): 9605–9614, https://doi.org/10.1021/acs.analchem.3c01319.

49. M. Cui, Y. Hu, Z. Zhang, et al., "Cyst Fluid Glycoproteins Accurately Distinguishing Malignancies of Pancreatic Cystic Neoplasm," *Signal Transduction and Targeted Therapy* 8 (2023): 406, https://doi.org/10.1038/s41392-023-01645-8.

50. N. Welch, S. S. Singh, R. Musich, et al., "Shared and Unique Phosphoproteomics Responses in Skeletal Muscle From Exercise Models and in Hyperammonemic Myotubes," *iScience* 25 (2022): 105325, https://doi.org/10.1016/j.isci.2022.105325.

51. C. Gutierrez, L. J. Salituro, C. Yu, et al., "Enabling Photoactivated Cross-Linking Mass Spectrometric Analysis of Protein Complexes by Novel MS-Cleavable Cross-Linkers," *Molecular & Cellular Proteomics* 20 (2021): 100084, https://doi.org/10.1016/j.mcpro.2021.100084.

52. G. Armony, E. Jacob, T. Moran, et al., "Cross-Linking Reveals Laminin Coiled-Coil Architecture," *Proceedings of the National Academy of Sciences* 113, no. 47 (2016) 13384–13389, https://doi.org/10.1073/pnas.1608424113.

53. M. Bassani-Sternberg, E. Bräunlein, R. Klar, et al., "Direct Identification of Clinically Relevant Neoepitopes Presented on Native Human Melanoma Tissue by Mass Spectrometry," *Nature Communications* 7 (2016): 13404, https://doi.org/10.1038/ncomms13404.

54. P. E. Geyer, N. A. Kulak, G. Pichler, L. M. Holdt, D. Teupser, and M. Mann, "Plasma Proteome Profiling to Assess Human Health and Disease," *Cell Systems* 2 (2016): 185–195, https://doi.org/10.1016/j.cels.2016.02.015.

55. Q. Wei, K. Li, L. Su, et al., "Plasma Proteomics Implicate Glutamic Oxaloacetic Transaminases as Potential Markers for Acute Myocardial Infarction," *Journal of Proteomics* 308 (2024): 105286, https://doi.org/10.1016/j.jprot.2024.105286.

56. U. H. Guzman, A. Martinez-Val, Z. Ye, et al., "Ultra-fast Label-Free Quantification and Comprehensive Proteome Coverage With Narrow-Window Data-Independent Acquisition," *Nature Biotechnology* 42 (2024): 1855–1866, https://doi.org/10.1038/s41587-023-02099-7.

57. D. Oliinyk and F. Meier, "Ion Mobility-Resolved Phosphoproteomics With Dia-PASEF and Short Gradients," *Proteomics* 23 (2023): 2200032, https://doi.org/10.1002/pmic.202200032.

58. J. Tüshaus, A. Sakhteman, S. Lechner, et al., "A Region-Resolved Proteomic Map of the Human Brain Enabled by High-Throughput Proteomics," *EMBO Journal* 42, no. 23 (2023): 114665, https://doi.org/10.15252/embj.2023114665.

59. Z. Wang, M. Mülleder, I. Batruch, et al., "High-Throughput Proteomics of Nanogram-Scale Samples With Zeno SWATH MS," *Elife* 11 (2022): 83947, https://doi.org/10.7554/eLife.83947.

60. A.-D. Brunner, M. Thielert, C. Vasilopoulou, et al., "Ultra-High Sensitivity Mass Spectrometry Quantifies Single-Cell Proteome Changes Upon Perturbation," *Molecular Systems Biology* 18 (2022): 10798, https://doi.org/10.15252/msb.202110798.

61. V. Demichev, L. Szyrwiel, F. Yu, et al., "dia-PASEF Data Analysis Using FragPipe and DIA-NN for Deep Proteomics of Low Sample Amounts," *Nature Communications* 13 (2022): 3944, https://doi.org/10.1038/s41467-022-31492-0.

62. C. Ctortecka, N. M. Clark, B. W. Boyle, et al., "Automated Single-Cell Proteomics Providing Sufficient Proteome Depth to Study Complex Biology Beyond Cell Type Classifications," *Nature Communications* 15 (2024): 5707, https://doi.org/10.1038/s41467-024-49651-w.

63. P. Skowronek, M. Thielert, E. Voytik, et al., "Rapid and In-Depth Coverage of the (Phospho-)Proteome With Deep Libraries and Optimal Window Design for Dia-PASEF," *Molecular & Cellular Proteomics* 21 (2022): 100279, https://doi.org/10.1016/j.mcpro.2022.100279.

64. S. Mukherjee, A. Jankevics, F. Busch, et al., "Oxonium Ion–Guided Optimization of Ion Mobility–Assisted Glycoproteomics on the timsTOF Pro," *Molecular & Cellular Proteomics* 22 (2023): 100486, https://doi.org/10.1016/j.mcpro.2022.100486.

65. Y. Hao, M. Chen, X. Huang, H. Xu, P. Wu, and S. Chen, "4D-diaXLMS: Proteome-Wide Four-Dimensional Data-Independent Acquisition Workflow for Cross-Linking Mass Spectrometry," *Analytical Chemistry* 95 (2023): 14077–14085, https://doi.org/10.1021/acs.analchem.3c02824.

66. C. H. Ihling, L. Piersimoni, M. Kipping, and A. Sinz, "Cross-Linking/Mass Spectrometry Combined With Ion Mobility on a timsTOF Pro Instrument for Structural Proteomics," *Analytical Chemistry* 93 (2021): 11442–11450, https://doi.org/10.1021/acs.analchem.1c01317.

67. C. N. Fuller, L. Valadares Tose, F. N. L. Vitorino, et al., "Bottom-Up Histone Post-Translational Modification Analysis Using Liquid Chromatography, Trapped Ion Mobility Spectrometry, and Tandem Mass Spectrometry," *Journal of Proteome Research* 23 (2024): 3867–3876, https://doi.org/10.1021/acs.jproteome.4c00177.

68. H. Zhang and D. Bensaddek, "Optimized Time-Segmented Acquisition Expands Peptide and Protein Identification in TIMS-TOF Pro Mass Spectrometry," *Journal of Proteome Research* 24 (2025): 526–536, https://doi.org/10.1021/acs.jproteome.4c00690.

69. M. Iwasaki, R. Nishimura, T. Yamakawa, Y. Miyamoto, T. Tabata, and M. Narita, "Differences in Uniquely Identified Peptides Between ddaPASEF and diaPASEF," *Cells* 13 (2024): 1848, https://doi.org/10.3390/cells13221848.

70. J. C. Rojas Echeverri, F. Hause, C. Iacobucci, et al., "A Workflow for Improved Analysis of Cross-Linking Mass Spectrometry Data Integrating Parallel Accumulation-Serial Fragmentation With MeroX and Skyline," *Analytical Chemistry* 96 (2024): 7373–7379, https://doi.org/10.1021/acs.analchem.4c00829.

71. D. Gomez-Zepeda, D. Arnold-Schild, J. Beyrle, et al., "Thunder-DDA-PASEF Enables High-Coverage Immunopeptidomics and Is Boosted by MS2Rescore With MS2PIP timsTOF Fragmentation Prediction Model," *Nature Communications* 15 (2024): 2288, https://doi.org/10.1038/s41467-024-46380-y.

72. N. Hoenisch Gravel, A. Nelde, J. Bauer, et al., "TOFIMS Mass Spectrometry-Based Immunopeptidomics Refines Tumor Antigen Identification," *Nature Communications* 14 (2023): 7472, https://doi.org/10.1038/s41467-023-42692-7.

73. M. Wahle, M. Thielert, M. Zwiebel, P. Skowronek, W.-F. Zeng, and M. Mann, "IMBAS-MS Discovers Organ-Specific HLA Peptide Patterns in Plasma," *Molecular & Cellular Proteomics* 23 (2024): 100689, https://doi.org/10.1016/j.mcpro.2023.100689.

74. J. Xiao, K. Frenia, K. C. Garwood, J. Kimmel, and L. T. Labriola, "High-Throughput Tear Proteomics via In-Capillary Digestion for Biomarker Discovery," *International Journal of Molecular Sciences* 25 (2024): 12239, https://doi.org/10.3390/ijms252212239.

Supporting Information

Additional supporting information can be found online in the Supporting Information section.

Supporting File 1: Tryptic digest parameters for the deep learning models AlphaPeptDeep and DeepCollisionalCrossSection (Table S1); library containing 404,935 unmodified peptides and their predicted m/z, z, RT, and CCS/z values (Table S2); diagram depicting how the filtering steps in the m/z, CCS/z, and LC dimensions were executed in the R code (Figure S1); experimentally measured mobility peak width distributions for TIMS and SLIM (Figure S2); arrival time ranges used to extract spectra with 1% or 5% mobility isolation widths (Figure S3); simulated chimeric frequency across all examined instrumentmodes (Figure S4); MS1 spectra associated with MS2 spectra from Figure 5 (Figure S5); comparison of specificity achieved with all instrument modes in experimental data (Figure S6). **Supporting File 2**: Library of predicted peptide *m/z*'s, normalized retention times, and CCS/z values (pmic70084-sup-0002-TableS2.tsv).